

Critical conditions for the buoyancy-driven detachment of a wall-bound pendant drop

A. Lamorgese and R. Mauri

Citation: *Physics of Fluids* **28**, 032103 (2016); doi: 10.1063/1.4942118

View online: <http://dx.doi.org/10.1063/1.4942118>

View Table of Contents: <http://scitation.aip.org/content/aip/journal/pof2/28/3?ver=pdfcov>

Published by the AIP Publishing

Articles you may be interested in

[Inertia-driven particle migration and mixing in a wall-bounded laminar suspension flow](#)

Phys. Fluids **27**, 123304 (2015); 10.1063/1.4936402

[Axisymmetric model of drop spreading on a horizontal surface](#)

Phys. Fluids **27**, 092103 (2015); 10.1063/1.4930813

[Oscillations of a sessile droplet in open air](#)

Phys. Fluids **25**, 112106 (2013); 10.1063/1.4829025

[The possible equilibrium shapes of static pendant drops](#)

J. Chem. Phys. **133**, 144707 (2010); 10.1063/1.3494041

[Buoyancy-driven viscous interaction of a rising drop with a smaller trailing drop](#)

Phys. Fluids **11**, 1016 (1999); 10.1063/1.869973



CiSE is already at
your fingertips...



In the IEEE Xplore and
AIP library packages.

Critical conditions for the buoyancy-driven detachment of a wall-bound pendant drop

A. Lamorgese and R. Mauri

Department of Civil and Industrial Engineering, University of Pisa, Largo Lazzarino 1, 56122 Pisa, Italy

(Received 29 October 2014; accepted 3 February 2016; published online 1 March 2016)

We investigate numerically the critical conditions for detachment of an isolated, wall-bound emulsion droplet acted upon by surface tension and wall-normal buoyancy forces alone. To that end, we present a simple extension of a diffuse-interface model for partially miscible binary mixtures that was previously employed for simulating several two-phase flow phenomena far and near the critical point [A. G. Lamorgese *et al.* “Phase-field approach to multiphase flow modeling,” *Milan J. Math.* **79**(2), 597–642 (2011)] to allow for static contact angles other than 90° . We use the same formulation of the Cahn boundary condition as first proposed by Jacqmin [“Contact-line dynamics of a diffuse fluid interface,” *J. Fluid Mech.* **402**, 57–88 (2000)], which accommodates a cubic (Hermite) interpolation of surface tensions between the wall and each phase at equilibrium. We show that this model can be successfully employed for simulating three-phase contact line problems in stable emulsions with nearly immiscible components. We also show a numerical determination of critical Bond numbers as a function of static contact angle by phase-field simulation. © 2016 AIP Publishing LLC. [<http://dx.doi.org/10.1063/1.4942118>]

I. INTRODUCTION

The objective of this research is to investigate the influence of static contact angles other than 90° on the buoyancy-driven detachment of an isolated emulsion droplet initially adhering to a wall under gravitational forcing, as a sequel to our previous study of Marangoni migration of a wall-bound drop in a temperature gradient,¹ wherein numerical simulations with a static contact angle of 90° were presented showing the existence of a critical gradient strength for detachment and subsequent migration to the hot wall, for an isolated drop initially adhering to the cold wall. In this work, we intend to study the mechanics of buoyancy-driven detachment in greater detail by determining the critical Bond number as a function of static contact angle. In fact, although the buoyancy-driven detachment of oily deposits (and liquid emulsion droplets in particular) from a solid substrate is of considerable interest in many industrial applications, due to the complexity of the removal process and the large variations in soils and substrates encountered, the details of the detachment process remain poorly understood and have long been the subject of active research.

Experimentally, in view of their relevance to detergency applications, a number of studies have been carried out on the detachment of liquid emulsion droplets from a solid substrate. In fact, since detergency is by far the largest single use for surfactants, early studies were conducted to investigate the principal mechanisms of oil drop removal from a solid substrate in aqueous surfactant solutions, together with their dependence on the relevant physico-chemical factors which control the efficiency of the cleaning process.^{2–8} Three main mechanisms were identified,^{8–12} i.e., emulsification, roll-up, and solubilization. Subsequent experiments have been performed to investigate different driving factors leading to a sequence of stages in the detachment process as well as the effects of temperature and a possible role of line tension.^{13,14} Of late, a series of (mainly) experimental studies have been focused on the inability of the above soil removal mechanisms to address complex fluid formulations of the soil deposits, such as those consisting of colloidal fluids containing nanometer-sized particles or surfactant micelles. In these cases, it has been shown that the disjoining pressure that results from the sub-microscale ordering of such nanoparticles or micelles has a

first-order controlling influence on the detachment process. Therefore, this has been recognized as a new mechanism of detergency.^{18–21}

On the numerical side, in an effort to investigate accuracy and limitations in the above explanations of the detergency mechanisms, some recent molecular dynamics simulations have looked into the nanometer-scale details and successive stages of the detachment process,^{15,16} as a result of these studies, for example, the roll-up mechanism has been traced to a shrinking of the three-phase contact line, which, in turn, is caused by the molecular diffusion of water molecules in-between an oil drop and the solid substrate.^{13,15,17}

Although experiments and simulations on the buoyancy-driven detachment of liquid emulsion droplets from solid substrates have been carried out in the past, none of those previous studies has addressed the critical Bond number as a function of the relevant nondimensional parameters systematically. In fact, in addition to the works cited above, a number of theoretical, numerical, and experimental investigations have been focused on the influence of a shear flow on the conditions for drop removal from solid surfaces,^{22–28} neglecting the more fundamental case of a pendant drop acted upon by surface tension and wall-normal buoyancy forces alone. At least in part, one reason for this neglect can be ascribed to the fact that the classical fluid dynamic formulation of incompressible two-phase flow with a dynamic contact line encounters a stress singularity which can only be resolved by replacing the no-slip boundary condition for the Navier-Stokes equation with a slip condition based on a tunable length. In this work, we investigate three-phase contact line problems using a diffuse-interface model, which circumvents the non-integrable stress singularity of the sharp-interface formulation and avoids physical property and dynamic variable discontinuities at geometrically complex moving interfaces. Instead, it treats the interfaces as having non-zero thickness and, as a result, all physical quantities vary continuously across the interfacial volume, a layer of finite (sub-micron scale) thickness. Another advantage of the diffuse-interface method is that it directly relates short-scale modifications of the hydrodynamic theory to molecular interactions. Accordingly, this method offers a continuum approach to resolving hydrodynamic singularities and may provide an excellent comparison with molecular-dynamic-type simulations of such singular phenomena.

Although the critical Bond number for buoyancy-driven detachment as a function of static contact angle has been addressed previously by numerical integration of the Young-Laplace equation,^{29–31} to our knowledge computations of that dependence based on a phase-field model have not been presented in the literature before and constitute the principal result reported herein. An outline of the remainder of this paper is as follows. The governing equations and numerical methods are briefly outlined in Secs. II and III, respectively. Then in Sec. IV, we show the results of numerical simulations of buoyancy-driven detachment and the determination of critical Bond numbers as a function of static contact angle. Finally, in Sec. V, a few conclusions are drawn.

II. THE GOVERNING EQUATIONS

Although the diffuse-interface model was originally developed to describe the near-critical behavior of single-component fluids and partially miscible binary mixtures,^{32,33} recently a number of phase-field formulations have been applied to interfacial flows far from criticality.^{1,34–37} In this work, 3D simulation results are employed to investigate predictions of buoyancy-driven detachment of liquid droplets from a solid substrate for stable emulsions with nearly immiscible components using a phase-field model for partially miscible binary mixtures far from the critical point.

Under isothermal conditions, the motion of a regular binary mixture with partially miscible components (where such components are assumed to have equal densities, viscosities and molecular weights) at low Reynolds number is described by the generalized Cahn-Hilliard and Stokes equations,^{38–41}

$$\partial_t \phi + \nabla \cdot \phi \mathbf{u} = -\nabla \cdot \mathbf{J}_\phi, \quad (1)$$

$$\nabla p = \eta \nabla^2 \mathbf{u} + \mathbf{F}_\phi + \mathbf{F}_g, \quad (2)$$

$$\nabla \cdot \mathbf{u} = 0. \quad (3)$$

Here, \mathbf{u} is the mass-averaged velocity, ϕ is the mass fraction, while \mathbf{J}_ϕ , \mathbf{F}_ϕ , and \mathbf{F}_g denote the volume flux and the Korteweg and buoyancy forces, respectively. In particular, the volume flux is proportional to the gradient of the chemical potential difference through the relation^{42,43}

$$\mathbf{J}_\phi = -D\phi(1-\phi)\nabla\tilde{\mu}, \quad (4)$$

where D is the molecular diffusivity while $\tilde{\mu}$ is the chemical potential difference, defined as $\tilde{\mu} = \delta(\tilde{g}/RT)/\delta\phi$. Here, \tilde{g} denotes the molar Gibbs free energy of mixing for a non-homogeneous mixture at temperature T and pressure P ,⁴⁴

$$\tilde{g} = RT[\phi \log \phi + (1-\phi) \log(1-\phi)] + RT\Psi\phi(1-\phi) + \frac{1}{2}RTa^2|\nabla\phi|^2, \quad (5)$$

with R , Ψ , and a denoting the universal gas constant, the Margules parameter, and a characteristic sub-microscopic length, respectively. In previous works, we have shown that this model can describe a number of two-phase flow phenomena both far and near the critical point, including phase separation by spinodal decomposition,³⁸ mixing of viscous binary liquid mixtures,⁴⁰ nucleation,³⁹ enhanced heat transport,⁴⁵ as well as Marangoni migration of isolated emulsion droplets in a temperature gradient.¹ In particular, when the mixture is brought from the single-phase region to the unstable range of its phase diagram, phase separation occurs ending with two coexisting phases separated by a sharp interface. At this point, a surface tension can be defined as the energy stored in the unit area of the interface,

$$\sigma = \frac{\rho RT a^2}{2M_W} \int |\nabla\phi|^2 d\ell = \frac{\rho RT a}{M_W} \mathcal{K}, \quad (6)$$

where \mathcal{K} is a dimensionless magnitude of the line integral of the square gradient component of the free energy for an interface profile at equilibrium. Using Hamilton's principle (and therefore neglecting all dissipative terms), the Korteweg force can be shown to be equal to the generalized gradient of the free energy,^{40,46}

$$\mathbf{F}_\phi = \frac{\rho}{M_W} \frac{\delta\tilde{g}}{\delta\mathbf{r}} = \frac{\rho RT}{M_W} \tilde{\mu} \nabla\phi. \quad (7)$$

In particular, at the late stages of phase separation, after the mixture has developed well-defined phase interfaces, this body force reduces to the more conventional surface tension.^{47,48} Therefore, being proportional to $\tilde{\mu} = \tilde{\mu}_A - \tilde{\mu}_B$, which is identically zero at local equilibrium, \mathbf{F}_ϕ can be thought of as a non-equilibrium capillary force. Note that \mathbf{F}_ϕ can be recast in the form

$$\mathbf{F}_\phi = -\phi \nabla\psi, \quad (8)$$

where $\psi = \frac{\rho RT}{M_W} \tilde{\mu}$. Hence, it becomes clear that the Korteweg force can be considered as a potential force. In fact, we can include into ψ any contributions due to other potential forces, as is the case, e.g., with buoyancy in the Boussinesq, quasi-incompressible approximation. That is also the case with the strictly isopycnic mixtures reported on in this work, where the buoyant force takes the form

$$\mathbf{F}_g = \rho \mathbf{g}(\phi - \langle\phi\rangle), \quad (9)$$

with the brackets denoting a volume average. This expression can be interpreted to include a uniform pressure gradient that has been superimposed in the $\hat{\mathbf{g}}$ direction, which guarantees a zero mean (species) volume flux.⁴⁹ Accordingly, gravity effects based on (9) can be accounted for by simply adding the term $V_{ext} = -\rho \mathbf{g} \cdot \mathbf{x}$ to ψ in Eq. (8). Note that for confined systems such as those considered in this work, wettability effects are normally present and must be taken into account. Such effects can be accounted for in our phase-field formulation by introducing the simplest additional surface contribution to the free energy functional, which is based on the assumption that wettability is a local quantity, solely depending on the local concentration of the two-phase fluid at the wall.⁵⁰ For clarity, we show below the same derivation of the Cahn boundary condition that has been presented elsewhere.⁵¹ The starting point is a statement of the Gibbs free energy of mixing that accounts for wettability effects,

$$\tilde{g}[\phi] = \frac{\rho}{M_W} \int_V \left[\Delta g_{th}(\phi) + \frac{1}{2} RT a^2 |\nabla\phi|^2 \right] d^3\mathbf{x} + \int_{\partial V} \left[-\frac{\rho RT a^2}{2M_W} \hat{\mathbf{n}} \cdot \phi \nabla\phi + g_s(\phi) \right] d^2\mathbf{x}, \quad (10)$$

where Δg_{th} is the molar thermodynamic Gibbs free energy of mixing [i.e., the sum of the first and second terms on the RHS of Eq. (5)], while g_s is the wall free energy per unit surface. Accordingly, taking the variation of this free energy functional yields

$$\delta \tilde{g} = \int_V \left[\frac{\rho}{M_W} \Delta g'_{th}(\phi) - \frac{\rho R T a^2}{M_W} \nabla^2 \phi \right] \delta \phi d^3 \mathbf{x} + \int_{\partial V} \left[\frac{\rho R T a^2}{2 M_W} \hat{\mathbf{n}} \cdot \nabla \phi + g'_s(\phi) \right] \delta \phi d^2 \mathbf{x} = 0, \quad (11)$$

where $\hat{\mathbf{n}}$ is the unit normal outward from the fluid domain. Setting $\delta \phi = 0$ in the bulk, Eq. (11) reduces to a minimization of the surface integral, leading to the following boundary condition:⁵⁰

$$\hat{\mathbf{n}} \cdot \nabla \phi = -\frac{2\mathcal{K}}{\sigma a} g'_s(\phi), \quad (12)$$

where \mathcal{K} has been defined through Eq. (6). For this relation to be useful as a boundary condition for the Cahn-Hilliard equation, modeling assumptions for g_s have to be introduced. The simplest such model is a linear interpolation of the surface tensions between the wall and each phase at equilibrium,⁵¹ i.e.,

$$g_s(\phi) = \sigma_{\beta,s} + \frac{\Delta\sigma}{\Delta\phi_{eq}} (\phi - \phi_{eq}^\beta). \quad (13)$$

Here, $\Delta\phi_{eq} \equiv \phi_{eq}^\alpha - \phi_{eq}^\beta$ and $\Delta\sigma \equiv \sigma_{\alpha,s} - \sigma_{\beta,s}$ expresses the affinity of the wall to the equilibrium α phase, as compared to the equilibrium β phase. Although this choice of g_s results in a viable formulation of the Cahn boundary condition,⁵¹ in this work we rely on its “classical” formulation which is based on a cubic (Hermite) polynomial interpolation for g_s , as first proposed by Jacqmin.⁴⁸ In fact, it can be argued that as a consequence of considering values of θ other than 90° two Margules coefficients should be employed for modeling the surface energy at the wall,⁵² i.e.,

$$g_s(\phi) = g_s^{id}(\phi) + [\Psi_{\alpha,s}\phi + \Psi_{\beta,s}(1-\phi)]\phi(1-\phi), \quad (14)$$

where g_s^{id} is a linear interpolation as above [Eq. (13)]. Hence it becomes clear that any modeling expression which interpolates $\sigma_{\alpha,s}$ (at $\phi = \phi_{eq}^\alpha$) and $\sigma_{\beta,s}$ (at $\phi = \phi_{eq}^\beta$) should be based on a cubic expression in powers of ϕ , which is uniquely determined by the following conditions: (i) $g_s(\phi_{eq}^\alpha) = \sigma_{s,\alpha}$ and $g_s(\phi_{eq}^\beta) = \sigma_{s,\beta}$, (ii) $g'_s(\phi_{eq}^\alpha) = g'_s(\phi_{eq}^\beta) = 0$. Finally we obtain⁴⁸

$$g_s(\phi) = \sigma_{\beta,s} + \frac{\Delta\sigma}{(\Delta\phi_{eq})^3} (\phi - \phi_{eq}^\beta)^2 (3\phi_{eq}^\alpha - \phi_{eq}^\beta - 2\phi). \quad (15)$$

As a result, the RHS of (12) involves a factor of $\Delta\sigma/\sigma$ which can be handled by means of Young’s equation, $\cos \theta = -\Delta\sigma/\sigma$. This is an additional relation (lying outside of the diffuse-interface framework) that must be invoked to make the connection with the equilibrium contact angle θ . Consequently, Eq. (12) can be rearranged to the form

$$\hat{\mathbf{n}} \cdot \nabla \phi = -\frac{12\mathcal{K} \cos \theta}{a(\Delta\phi_{eq})^3} (\phi - \phi_{eq}^\alpha)(\phi - \phi_{eq}^\beta). \quad (16)$$

Note that the above formulation of the Cahn boundary condition relies on an accurate (and independent) specification of the surface tension coefficient \mathcal{K} . As a practical matter, any uncertainty in the relation employed for evaluating σ (equivalent to an approximate choice of \mathcal{K}) translates into an uncertain specification of equilibrium contact angle. In fact, from an order-of-magnitude estimate for σ based on Eq. (6) in the vicinity of the critical point, we obtain $\mathcal{K} \sim (\Delta\phi_{eq})^2 \sqrt{\Psi - 2}$, which overestimates the actual value of \mathcal{K} found in simulation and this leads to a misrepresentation of the static contact angle as compared to its actual (prescribed) value. Therefore, the value of \mathcal{K} in our numerical implementation was calculated from its definition, i.e., a numerically determined line integral of the square gradient component of the Gibbs free energy of mixing for an interface profile at equilibrium. Note that \mathcal{K} depends on Ψ as well as on a (dimensionless) drop size. In fact, values of \mathcal{K} were also obtained based on a “dynamic” surface tension evaluation, where the line integral just mentioned is performed at each time step in simulation. Incidentally, we found that the latter “dynamic” evaluation of \mathcal{K} yields values that are quite close to its “static” determination, at least as long as the isolated drop is distant (in simulation time)

from a pinchoff event. In conclusion, we note that integrating the Cahn-Hilliard equation requires specification of two additional boundary conditions and those are provided by the no-flux condition $\hat{\mathbf{n}} \cdot \mathbf{J}_\phi = 0$ (with $\hat{\mathbf{n}}$ denoting a unit vector in the wall normal direction), which can be recast in the form

$$\frac{\partial^3 \phi}{\partial n^3} = \frac{1}{a^2} \frac{\partial \phi}{\partial n} \left[\frac{1}{\phi(1-\phi)} - 2\Psi \right] - \nabla_s^2 \frac{\partial \phi}{\partial n}, \quad (17)$$

where $\nabla_s = (\mathbf{I} - \hat{\mathbf{n}}\hat{\mathbf{n}})\nabla$ is the surface gradient (all quantities shown being computed at the wall).

III. NUMERICAL METHODS

The governing equations (in dimensionless form) can be rewritten as follows:

$$\begin{aligned} (\partial_t - \nabla^2)\phi = & -\nabla^2 \left\{ \phi(1-\phi) \left[2\Psi\phi + \left(\frac{a}{h}\right)^2 \nabla^2 \phi \right] \right\} \\ & + \nabla \cdot \left\{ \left[2\Psi\phi + \left(\frac{a}{h}\right)^2 \nabla^2 \phi \right] (1-2\phi)\nabla\phi - \alpha\phi\mathbf{u} \right\}, \end{aligned} \quad (18)$$

$$\left(\frac{a}{h}\right)^2 \nabla^2 \mathbf{u} = \mathbb{P}(\nabla)\phi\nabla \left[\tilde{\mu} - \left(\frac{a}{d}\right)^2 \frac{\mathcal{K}Bo}{\Delta\phi_{eq}} \frac{h}{a} y \right], \quad (19)$$

where all lengths and times are scaled by h and h^2/D , respectively, with h denoting the channel half-width. In Eq. (18), α denotes the fluidity coefficient,⁵³ defined as

$$\alpha \equiv \frac{RTa^2}{M_W \nu D}. \quad (20)$$

This dimensionless parameter can be shown to be the same as an inverse capillary number,⁵⁴ while, on the other hand, it can also be interpreted as a Peclet number,^{38–41} i.e., the ratio of convective to diffusive mass fluxes in the Cahn-Hilliard equation. Equation (19) can be seen as a static constraint on the (dimensionless) velocity field, i.e., at each instant in time the velocity can be determined once the concentration field is known [so that the \mathbf{u} -dependence on the RHS of (18) can be formally dropped]. The projection operator, $\mathbb{P}_{ij}(\nabla) \equiv \delta_{ij} - \nabla^2 \partial_{ij}^2$, in Eq. (19) guarantees a solenoidal velocity at all times. Finally, the relative importance of buoyancy compared to surface tension forces appears as a Bond number on the RHS of Eq. (19), which has been defined as $Bo \equiv (d/l_c)^2$, where d is the initial droplet diameter while $l_c \equiv \sqrt{\sigma/g\rho\Delta\phi_{eq}}$ is a capillary length.

Numerical methods are the same as in our previous works.^{1,41} We only summarize below the necessary changes to our numerical algorithm that allow the implementation of our formulation of the Cahn boundary condition [Eq. (16)] together with the no-flux condition [Eq. (17)]. Now, as can be seen by inspection from Eqs. (16) and (17), the boundary conditions on the first and third-order normal derivatives of ϕ at the wall depend on ϕ itself as well as on the surface gradient (squared) and surface Laplacian of ϕ at the wall. Therefore, at each substep of a second-order Runge-Kutta/Crank-Nicolson scheme,⁵⁵ one has to iteratively solve for ϕ until those normal derivatives at the wall no longer change as the number of subiterations grows unbounded (as a practical matter, the subiterations are stopped as soon as a limit number is reached). In our code, this has been implemented as an exit condition. In particular, at each substep the third-order derivative at the wall is taken to have converged after J subiterations if, for some prescribed tolerance, the following condition

$$\left\| \frac{\partial^3 \phi}{\partial y^3}[\phi^{J-1}] - \frac{\partial^3 \phi}{\partial y^3}[\phi^J] \right\| < tol \quad (21)$$

holds in some suitable norm (production runs were conducted using the vector 1-norm and $tol = 10^{-4}$). It is worth noting that in our previous work⁴¹ homogeneous boundary conditions on the first- and third-order y -derivatives of the concentration at the wall had been imposed using an influence-matrix technique.⁵⁶ In this work, inhomogeneous conditions [such as those in Eqs. (16) and (17)] have been dealt with in either one of two ways: (i) by interpolating the inhomogeneous

boundary conditions as a body force so that our previous influence matrix solver for homogeneous boundary conditions could still be utilized,⁵⁷ and (ii) by making changes to the influence matrix solver that allow for inhomogeneous boundary conditions. In fact, although a modified influence matrix solver for inhomogeneous conditions was implemented in our code, in our production runs we chose the former method of boundary condition interpolation as a body force due to its lower complexity [since most results in this paper are from simulations requiring (each one) on the order of 10^6 aggregate subiterations].

IV. RESULTS AND DISCUSSION

Numerical results from simulations in a channel-like geometry are now described. In what follows, the static contact angle dependence of the critical Bond number will be discussed by first using dimensionless parameters that are readily accessible in our numerical setup. Subsequently, using a change of variables that dependence will also be presented in terms of standard macroscopic quantities (i.e., θ and Bo). In fact, the actual dimensionless groups that appear in the governing equations [Eqs. (18) and (19)] after diffusive scaling of the Stokes/Cahn-Hilliard system are the fluidity coefficient [Eq. (20)] and a dimensionless magnitude of the buoyancy force, defined as

$$\mathcal{G} \equiv \frac{g\Delta\phi_{eq}d^3}{\alpha\nu D} = \frac{GaSc}{\alpha}, \quad (22)$$

where $Ga \equiv g\Delta\phi_{eq}d^3/\nu^2$ is a Galileo number while $Sc \equiv \nu/D$ is the Schmidt number. Hence it becomes clear that the critical conditions for detachment of an isolated, wall-bound drop can be uniquely identified through the dependence

$$\mathcal{G}_c = fn(\Delta\tilde{\sigma}), \quad (23)$$

where $\Delta\tilde{\sigma}$ is the dimensionless surface tension difference at the wall, i.e.,

$$\Delta\tilde{\sigma} \equiv \frac{\Delta\sigma}{\rho RTa/M_W}. \quad (24)$$

Note that, based on our previous definitions, we have

$$\cos\theta = -\frac{\Delta\tilde{\sigma}}{\mathcal{K}} \quad \text{and} \quad Bo = \mathcal{G}\frac{a/d}{\mathcal{K}}. \quad (25)$$

The presence of \mathcal{K} in the denominator of both of these relations (due to a reciprocal dependence on σ when rearranged in terms of dimensional quantities) indicates that θ and the Bond number are not readily available in our numerical setup and can only be evaluated after a numerical determination of \mathcal{K} (further addressed below). Simulations of buoyancy-driven detachment were carried out in a computational domain of size $L_x = L_z = \frac{\pi}{2}N\frac{a}{\sqrt{\Psi}}$, $L_y = N\frac{a}{\sqrt{\Psi}}$ ($N = 64$), with a pendant droplet (having a radius equal to $5.8a$) of the minority phase embedded in a continuous phase (with both phases at equilibrium), corresponding to $\langle\phi\rangle = 0.1127$. We chose $\Psi = 2.7$ (corresponding to equilibrium mass fractions $\phi_{eq}^\beta = 0.1069$ and $\phi_{eq}^\alpha = 0.8929$) and $\alpha = 100$, yielding results that could be considered as roughly representative of a binary mixture with nearly immiscible components. Interface profiles were interpolated using ~ 3 grid points (based on an estimate of the actual interface thickness as $\lambda \equiv a/\sqrt{\Psi-2}$). Additional numerical tests to investigate numerical convergence upon grid refinement as well as the dependence of our numerical results on the resolution requirements for interface profiles are further addressed below. In fact, a discussion of the minimum number of grid points for resolving the interfacial thickness had already been presented in a previous publication.³⁹

First, we ran a test case to make sure that, in the absence of gravity, a drop initially placed on the solid substrate with a contact angle of 90° would relax towards an equilibrium state corresponding to a prescribed contact angle $\theta^* \neq 90^\circ$. Using the following geometric relation⁵⁸

TABLE I. Final values of contact angle $\theta_m(\tilde{\phi})$ ($\tilde{\phi}$ being the chosen mass fraction isosurface) as a function of prescribed contact angle (θ^*) in the absence of gravity.

θ^*	30°	45°	60°	90°	120°	150°
$\theta_m(0.5)$	38.9°	45.9°	57.2°	90°	117.7°	142.8°
$\theta_m(0.75)$	35.3°	35.3°	55.8°	90°	124.7°	166.2°

$$\tan \theta_m = \frac{bW}{\frac{W^2}{4} - b^2}, \quad (26)$$

where W is the drop width while b is its height (measured in the symmetry plane $z = L_z/2$), values of final contact angle θ_m were computed for each prescribed contact angle as reported in Table I. As can be seen, all final values are in reasonable agreement with the corresponding prescribed values though some deviations are apparent, particularly as $|\theta^* - 90^\circ|$ increases. Note that each final value of contact angle also depends on the choice of ϕ -isosurface employed for measuring b and W . As a result, the measured values slightly change when using the $\tilde{\phi} = 0.75$ isosurface as compared to those corresponding to $\tilde{\phi} = 0.5$.

At first, values of dimensionless surface tension difference were chosen in a discrete set $\Delta\tilde{\sigma} = \{-8.68 \times 10^{-2}, -8.38 \times 10^{-2}, -7.52 \times 10^{-2}, -6.14 \times 10^{-2}, -4.34 \times 10^{-2}, 0, 2.97 \times 10^{-2}, 7.52 \times 10^{-2}, 8.68 \times 10^{-2}\}$. For each such value, we ran simulations for different (dimensionless) buoyancy magnitudes to identify the critical magnitude corresponding to a pinchoff event. This is documented in Fig. 1 showing snapshots of mass fraction isosurfaces at different (nondimensional) times for three cases corresponding to detachment with $\Delta\tilde{\sigma} < 0$ and $\Delta\tilde{\sigma} > 0$ and to no detachment with $\Delta\tilde{\sigma} < 0$ (recall that $\Delta\tilde{\sigma} > 0$ corresponds to an obtuse contact angle). In particular, we found $\Delta\tilde{\sigma} = 8.68 \times 10^{-2}$ as the smallest (positive) surface tension difference for which a drop would detach from the wall under a zero gravity magnitude. This value of surface tension difference can be interpreted (in dimensional terms) as defining the reference surface tension needed for introducing θ as an alternative abscissa in place of $\Delta\tilde{\sigma}$ (i.e., $\Delta\sigma = \sigma$ with $\mathcal{G}_c = 0$ corresponds to $\theta = 180^\circ$).

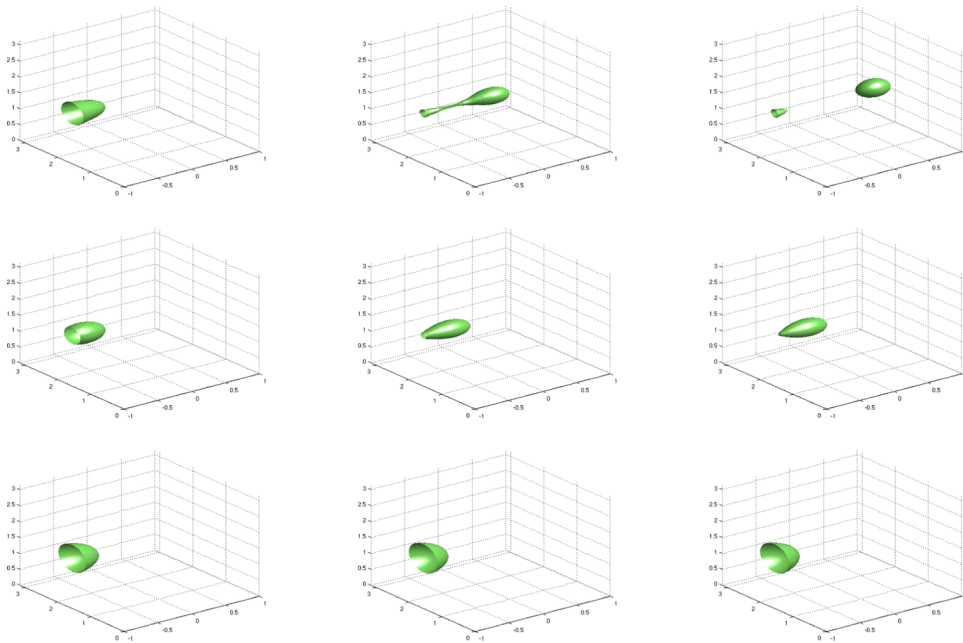


FIG. 1. Snapshots of mass fraction isosurfaces at different (nondimensional) times $t = 5 \times 10^{-3}$, 3.8×10^{-2} , and 4.3×10^{-2} from phase-field computations with $\Psi = 2.7$, $\alpha = 100$, and $\langle \phi \rangle = 0.1127$ on a $64 \times 65 \times 64$ grid corresponding to $\Delta\tilde{\sigma} = -7.52 \times 10^{-2}$ with $\mathcal{G} = 1.6 \mathcal{G}_c$ (top row), $\Delta\tilde{\sigma} = 7.52 \times 10^{-2}$ with $\mathcal{G} = 1.5 \mathcal{G}_c$ (middle row), and $\Delta\tilde{\sigma} = -4.34 \times 10^{-2}$ with $\mathcal{G} = 0.8 \mathcal{G}_c$ (bottom row).

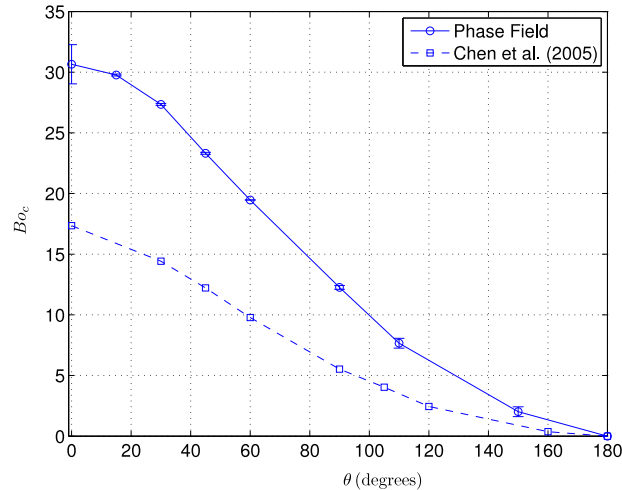


FIG. 2. Critical Bond numbers as a function of static contact angle from phase-field computations with $\Psi = 2.7$, $\alpha = 100$, and $\langle \phi \rangle = 0.1127$ on a $64 \times 65 \times 64$ grid (solid) vs. static stability analysis of equilibrium shapes obtained from the Young-Laplace equation (dashed).

Based on the first relation in (25), this then identifies the value $\mathcal{K}^* = 8.68 \times 10^{-2}$ for switching to a $Bo_c = fn(\theta)$ description. Interestingly, this value is not too far from the previously noted equilibrium determination of \mathcal{K} , i.e., $\mathcal{K}^* \approx 1.32\mathcal{K}_{eq}$. The corresponding values of θ are in the discrete set $\{0^\circ, 15^\circ, 30^\circ, 45^\circ, 60^\circ, 90^\circ, 110^\circ, 150^\circ, 180^\circ\}$. Hence we see that the cases shown in Fig. 1 correspond to detachment with $\theta < 90^\circ$ and $\theta > 90^\circ$ and to no detachment with $\theta < 90^\circ$.

For each value of $\theta < 90^\circ$, we found that for all Bond numbers larger than critical a partial detachment event, wherein a remnant drop remains attached to the solid substrate, occurs. In contrast, for $\theta > 90^\circ$, the shape of the interface at pinchoff is a single cone that detaches from the wall at its tip (which prevents the occurrence of a partial drop detachment), whereas for $\theta = 90^\circ$, we found that a Bond number much larger than critical corresponds to a partial drop detachment from the solid substrate, while for Bond numbers only slightly larger than critical, a complete detachment is achieved. These numerical results are summarized in Fig. 2, showing critical Bond numbers as a function of static contact angle. As a point of information, the error bars represent the limiting runs at which pinchoff did and did not occur. Note that, on average, more than 10 runs were required for each θ value in the set above in order to shrink the error bars to zero (i.e., to the extent shown in Fig. 2). In fact, for a given contact angle the number of time steps to a pinchoff event increases as the critical condition is approached, i.e., as $\xi \rightarrow 0$ (where $\xi \equiv Bo/Bo_c - 1$ is a measure of the distance to the critical condition at a fixed contact angle). For some cases with the smallest error bars, supercritical Bond numbers corresponding to $\xi \approx 3 \times 10^{-4}$ were achieved in simulation. Each one of these cases required over 10^5 time steps to reveal a pinchoff event (based on the aforementioned $64 \times 65 \times 64$ grid), i.e., over a million aggregate subiterations to complete (corresponding approximately to 90 h of wall-clock time on a serial processor). In fact, for a given convergence tolerance, the number of subiterations was found to increase with $|\theta - 90^\circ|$.

Briefly, we looked at the grid size dependence of our numerically determined critical Bond numbers by checking that we could obtain essentially the same critical Bond number as above (at $\theta = 90^\circ$) using both a smaller initial drop radius ($4.2a$) and computational domain size having $48 \times 49 \times 48$ grid points (resulting in the same $\langle \phi \rangle$ value as above). Based on this last grid size, a value of 12.23 results for the critical Bond number at $\theta = 90^\circ$, which is less than 1% off its value at $64 \times 65 \times 64$. Note that the error bars at $48 \times 49 \times 48$ were shrunk to the point where they fall within those corresponding to $64 \times 65 \times 64$. In fact, these values of $Bo_c(\theta = 90^\circ)$ for different grid sizes also correspond to different Cahn numbers so we ran additional simulations at $72 \times 73 \times 72$ having one additional grid point to resolve interface profiles (as compared to those at $48 \times 49 \times 48$) so that the Cahn numbers for the two grid sizes could be matched. A value of 12.32 results for

$Bo_c(\theta = 90^\circ)$, which is less than 1% off its value at $64 \times 65 \times 64$, though the error bar with the finest grid size is approximately 30% wider than with the original grid (i.e., $64 \times 65 \times 64$). We also looked at numerical convergence for the critical Bond number at a single value of $\theta > 90^\circ$. Using $48 \times 49 \times 48$ grid points, a value of 7.71 results for the critical Bond number at $\theta = 110^\circ$, which is less than 3% off its value at $64 \times 65 \times 64$.

Also shown in Fig. 2 are critical Bond numbers for axisymmetric droplets as a function of contact angle from sharp-interface equilibrium calculations based on Surface Evolver.³¹ As can be seen, these values are approximately half of those determined by phase-field simulation. We can only speculate on the factors leading to such a discrepancy, since a more precise assessment should be based on a large database of buoyancy-driven detachment simulations (missing in our case). It should be borne in mind that in all simulations reported herein, a drop of the minority phase displaces continuous phase fluid when settling in the gravity direction, and this creates a backflow in its vicinity which could tend to further hinder the detachment process as the backflow strength increases. Although the effects of a backflow are likely to be significant for Bond numbers much larger than the critical value at a given contact angle, based on the observation of an extremely slow process of detachment very near to the critical condition (i.e., for Bond numbers only slightly larger than critical), a backflow is expected to have a negligible influence on the critical Bond number. Another, more important, factor contributing to the discrepancy in Fig. 2 is the static stability analysis ignoring the dynamics of the detachment process. In particular, a sharp-interface description together with its assumption of constant surface tension are expected to fail in the necking regime of drop detachment, where a sharpening of concentration gradients in the necking region leads to an effective increase in (dynamic) surface tension [defined in Eq. (6)], ultimately leading to a reduced tendency to detachment or an increase in the critical Bond number. This is being looked at in more detail in a parallel investigation,⁵⁹ which is primarily concerned with interface shape at pinchoff and nonequilibrium surface tension during detachment of a wall-bound pendant drop. Results from those simulations confirm that for a pendant drop at pinchoff the nonequilibrium surface tension has a nonuniform distribution with peak values located at the advancing tip and in the necking region near the minimum neck radius. Thus, for a given capillary pressure between the two phases at equilibrium, the increase in the nonequilibrium surface tension at the moment of pinchoff will determine an almost flat interface shape at rupture, therefore retarding drop detachment (as compared to a sharp-interface description based on a constant surface tension). As a final note regarding the comparison in Fig. 2, it should be borne in mind that while our critical Bond number dependence refers to a strictly isopycnic system, the critical Bond numbers from Chen *et al.*³¹ address interfaces with a strong density contrast (such as, e.g., the air/water interface). Thus, surprisingly, we find a factor of 2 rather an order-of-magnitude discrepancy between our results and those from the sharp-interface analysis.

V. CONCLUSIONS

In this paper, results of 3D phase-field simulations of buoyancy-driven detachment of a pendant emulsion droplet have been presented with the main objective of determining the critical Bond number as a function of static contact angle. Starting from the basic conservation principles, we have shown that a diffuse-interface description of partially miscible, regular binary liquid mixtures far from the critical point can be successfully employed for simulating three-phase contact line problems in stable emulsions with nearly immiscible components. In addition, we have shown that the classical formulation of the Cahn boundary condition based on a cubic (Hermite) interpolation of surface tensions between the wall and each phase at equilibrium can be readily implemented in our numerical procedures. Also, we discussed changes to our numerical algorithm that include an iterative method of enforcing inhomogeneous boundary conditions within a semi-implicit temporal scheme for the Cahn-Hilliard equation.

Results of 3D computations have shown a characteristic monotonic behavior of the critical Bond number as a function of static contact angle. We argue that the discrepancy between our numerically determined static contact angle dependence of the critical Bond number and its

sharp-interface counterpart from a static stability analysis based on a numerical integration of the Young-Laplace equation can be explained in terms of (i) the inability of the sharp-interface analysis to describe the later stages of the detachment process and, in particular, the sharpening of concentration gradients leading to an effective increase in (dynamic) surface tension and critical Bond number, and (ii) a nonnegligible dependence on mean mass fraction of the critical Bond number at a given contact angle, due to a backflow which tends to hinder the detachment process as the backflow strength increases. However, that dependence cannot be properly addressed using the present dataset and is left for future work.

ACKNOWLEDGMENTS

Financial support provided by MIUR (Grant No. PGR10DN9YV) is gratefully acknowledged.

- ¹ A. G. Lamorgese and R. Mauri, "Liquid mixture convection during phase separation in a temperature gradient," *Phys. Fluids* **23**, 034102 (2011).
- ² A. M. Schwartz, "The physical chemistry of detergency," in *Surface and Colloid Science*, edited by E. Matijevic (Wiley, 1972), Vol. 5, pp. 195–244.
- ³ K. Dillan, E. Goddard, and D. McKenzie, "Oily soil removal from a polyester substrate by aqueous nonionic surfactant systems," *J. Am. Oil Chem. Soc.* **56**(1), 59–70 (1979).
- ⁴ M. Gum and E. Goddard, "Adsorption study of nonionic surfactants on polyester fibers," *J. Am. Oil Chem. Soc.* **59**(3), 142–145 (1982).
- ⁵ M. Aronson, M. Gum, and E. Goddard, "Behavior of surfactant mixtures in model oily-soil detergency studies," *J. Am. Oil Chem. Soc.* **60**(7), 1333–1339 (1983).
- ⁶ *Detergency: Theory and Technology*, edited by G. Cutler and E. Kissa (CRC Press, 1986).
- ⁷ K. H. Raney and C. A. Miller, "Optimum detergency conditions with nonionic surfactants: II. Effect of hydrophobic additives," *J. Colloid Interface Sci.* **119**(2), 539–549 (1987).
- ⁸ L. Thompson, "The role of oil detachment mechanisms in determining optimum detergency conditions," *J. Colloid Interface Sci.* **163**(1), 61–73 (1994).
- ⁹ C. A. Miller and K. H. Raney, "Solubilization-emulsification mechanisms of detergency," *Colloids Surf., A* **74**(2), 169–215 (1993).
- ¹⁰ A. W. Adamson and A. P. Gast, *Physical Chemistry of Surfaces*, 6th ed. (Wiley-Interscience, New York, 1997), Chap. XIII.
- ¹¹ A. W. Rowe, R. M. Counce, S. A. Morton III, M.-C. Hu, and D. W. DePaoli, "Oil detachment from solid surfaces in aqueous surfactant solutions as a function of pH," *Ind. Eng. Chem. Res.* **41**(7), 1787–1795 (2002).
- ¹² J. C. López-Montilla, M. A. James, O. D. Crisalle, and D. O. Shah, "Surfactants and protocols to induce spontaneous emulsification and enhance detergency," *J. Surfactants Deterg.* **8**(1), 45–53 (2005).
- ¹³ V. Kolev, I. Kochijashky, K. Danov, P. Kralchevsky, G. Broze, and A. Mehreteab, "Spontaneous detachment of oil drops from solid substrates: Governing factors," *J. Colloid Interface Sci.* **257**(2), 357–363 (2003).
- ¹⁴ P. A. Kralchevsky, K. D. Danov, V. L. Kolev, T. D. Gurkov, M. I. Temelska, and G. Brenn, "Detachment of oil drops from solid surfaces in surfactant solutions: Molecular mechanisms at a moving contact line," *Ind. Eng. Chem. Res.* **44**(5), 1309–1321 (2005).
- ¹⁵ Q. Liu, S. Yuan, H. Yan, and X. Zhao, "Mechanism of oil detachment from a silica surface in aqueous surfactant solutions: Molecular dynamics simulations," *J. Phys. Chem. B* **116**(9), 2867–2875 (2012).
- ¹⁶ P. Zhang, Z. Xu, Q. Liu, and S. Yuan, "Mechanism of oil detachment from hybrid hydrophobic and hydrophilic surface in aqueous solution," *J. Chem. Phys.* **140**(16), 164702 (2014).
- ¹⁷ R. Kao, D. Wasan, A. Nikolov, and D. Edwards, "Mechanisms of oil removal from a solid surface in the presence of anionic micellar solutions," *Colloids Surf.* **34**(4), 389–398 (1989).
- ¹⁸ D. T. Wasan and A. D. Nikolov, "Spreading of nanofluids on solids," *Nature* **423**, 156–159 (2003).
- ¹⁹ A. Chengara, A. D. Nikolov, D. T. Wasan, A. Trokhymchuk, and D. Henderson, "Spreading of nanofluids driven by the structural disjoining pressure gradient," *J. Colloid Interface Sci.* **280**(1), 192–201 (2004).
- ²⁰ D. Wasan, A. Nikolov, and K. Kondiparty, "The wetting and spreading of nanofluids on solids: Role of the structural disjoining pressure," *Curr. Opin. Colloid Interface Sci.* **16**(4), 344–349 (2011).
- ²¹ K. Kondiparty, A. Nikolov, S. Wu, and D. Wasan, "Wetting and spreading of nanofluids on solid surfaces driven by the structural disjoining pressure: Statics analysis and experiments," *Langmuir* **27**(7), 3324–3335 (2011).
- ²² V. Thoreau, B. Malki, G. Berthome, L. Boulange-Petermann, and J. Joud, "Physico-chemical and dynamic study of oil-drop removal from bare and coated stainless-steel surfaces," *J. Adhes. Sci. Technol.* **20**(16), 1819–1831 (2006).
- ²³ P. Dimitrakopoulos and J. Higdon, "Displacement of fluid droplets from solid surfaces in low-Reynolds-number shear flows," *J. Fluid Mech.* **336**, 351–378 (1997).
- ²⁴ P. Dimitrakopoulos and J. Higdon, "On the displacement of three-dimensional fluid droplets from solid surfaces in low-Reynolds-number shear flows," *J. Fluid Mech.* **377**, 189–222 (1998).
- ²⁵ A. Theodorakakos, T. Ous, M. Gavaises, J. Nouri, N. Nikolopoulos, and H. Yanagihara, "Dynamics of water droplets detached from porous surfaces of relevance to PEM fuel cells," *J. Colloid Interface Sci.* **300**(2), 673–687 (2006).
- ²⁶ A. Golpaygan and N. Ashgriz, "Multiphase flow model to study channel flow dynamics of PEM fuel cells: Deformation and detachment of water droplets," *Int. J. Comput. Fluid Dyn.* **22**(1-2), 85–95 (2008).
- ²⁷ S. Basu, K. Nandakumar, and J. H. Masliyah, "A model for detachment of a partially wetting drop from a solid surface by shear flow," *J. Colloid Interface Sci.* **190**(1), 253–257 (1997).

- ²⁸ V. Fréville, E. van Hecke, C. Ernenwein, A.-V. Salsac, and I. Pezron, "Effect of surfactants on the deformation and detachment of oil droplets in a model laminar flow cell," *Oil Gas Sci. Technol.* **69**(3), 435–444 (2014).
- ²⁹ J. Chatterjee, "Critical Eotvos numbers for buoyancy-induced oil drop detachment based on shape analysis," *Adv. Colloid Interface Sci.* **98**(3), 265–283 (2002).
- ³⁰ J. Chatterjee, "Shape analysis based critical Eotvos numbers for buoyancy-induced partial detachment of oil drops from hydrophilic surfaces," *Adv. Colloid Interface Sci.* **99**(2), 163–179 (2002).
- ³¹ Y. Chen, M. Bacich, C. Nardin, A. Sitorus, and M. M. Weislogel, "The shape and stability of wall-bound and wall-edge-bound drops and bubbles," *Microgravity Sci. Technol.* **17**(4), 14–24 (2005).
- ³² J. D. van der Waals, "The thermodynamic theory of capillarity under the hypothesis of a continuous variation of density," *Z. Phys. Chem. Stöchiom. Verwandtschaftsl.* **13**, 657–725 (1894) [translated and reprinted in *J. Stat. Phys.* **20**, 200–244 (1979)].
- ³³ J. W. Cahn and J. Hilliard, "Free energy of a nonuniform system. III. Nucleation in a two-component incompressible fluid," *J. Chem. Phys.* **31**, 688–699 (1959).
- ³⁴ R. Borcia and M. Bestehorn, "Phase-field simulations for drops and bubbles," *Phys. Rev. E* **75**(5), 056309 (2007).
- ³⁵ H. Ding and P. D. Spelt, "Onset of motion of a three-dimensional droplet on a wall in shear flow at moderate Reynolds numbers," *J. Fluid Mech.* **599**, 341–362 (2008).
- ³⁶ H. Ding, M. N. Gilani, and P. D. Spelt, "Sliding, pinch-off and detachment of a droplet on a wall in shear flow," *J. Fluid Mech.* **644**, 217–244 (2010).
- ³⁷ H. Liu, A. J. Valocchi, Y. Zhang, and Q. Kang, "Phase-field-based lattice Boltzmann finite-difference model for simulating thermocapillary flows," *Phys. Rev. E* **87**(1), 013010 (2013).
- ³⁸ A. G. Lamorgese and R. Mauri, "Phase separation of liquid mixtures," in *Nonlinear Dynamics and Control in Process Engineering*, edited by G. Continillo *et al.* (Springer, Rome, 2002), pp. 139–152.
- ³⁹ A. G. Lamorgese and R. Mauri, "Nucleation and spinodal decomposition of liquid mixtures," *Phys. Fluids* **17**, 034107 (2005).
- ⁴⁰ A. G. Lamorgese and R. Mauri, "Mixing of macroscopically quiescent liquid mixtures," *Phys. Fluids* **18**, 044107 (2006).
- ⁴¹ A. G. Lamorgese and R. Mauri, "Diffuse-interface modeling of phase segregation in liquid mixtures," *Int. J. Multiphase Flow* **34**(6), 987–995 (2008).
- ⁴² R. Mauri, R. Shinnar, and G. Triantafyllou, "Spinodal decomposition in binary mixtures," *Phys. Rev. E* **53**, 2613–2623 (1996).
- ⁴³ N. Vladimirova, A. Malagoli, and R. Mauri, "Diffusion-driven phase separation of deeply quenched mixtures," *Phys. Rev. E* **58**, 7691–7699 (1998).
- ⁴⁴ J. W. Cahn and J. Hilliard, "Free energy of a nonuniform system. I. Interfacial free energy," *J. Chem. Phys.* **28**, 258–267 (1958).
- ⁴⁵ D. Molin and R. Mauri, "Enhanced heat transport during phase separation of liquid binary mixtures," *Phys. Fluids* **19**, 074102 (2007).
- ⁴⁶ J. Lowengrub and L. Truskinovsky, "Quasi-incompressible Cahn-Hilliard fluids and topological transitions," *Proc. R. Soc. A* **454**, 2617–2654 (1998).
- ⁴⁷ D. Jasnow and J. Viñals, "Coarse-grained description of thermo-capillary flow," *Phys. Fluids* **8**, 660–669 (1996).
- ⁴⁸ D. Jacqmin, "Contact-line dynamics of a diffuse fluid interface," *J. Fluid Mech.* **402**, 57–88 (2000).
- ⁴⁹ R. Mauri, *Non-Equilibrium Thermodynamics in Multiphase Flows* (Springer, 2013).
- ⁵⁰ J. W. Cahn, "Critical point wetting," *J. Chem. Phys.* **66**(8), 3667–3672 (1977).
- ⁵¹ A. G. Lamorgese, D. Molin, and R. Mauri, "Phase-field approach to multiphase flow modeling," *Milan J. Math.* **79**(2), 597–642 (2011).
- ⁵² J. M. Smith and H. C. Van Ness, *Introduction to Chemical Engineering Thermodynamics*, 4th ed. (McGraw-Hill, Boston, 1987), p. 378.
- ⁵³ H. Tanaka and T. Araki, "Spontaneous double phase separation induced by rapid hydrodynamic coarsening in two-dimensional fluid mixtures," *Phys. Rev. Lett.* **81**, 389–392 (1998).
- ⁵⁴ N. Vladimirova, A. Malagoli, and R. Mauri, "Diffusiophoresis of two-dimensional liquid droplets in a phase-separating system," *Phys. Rev. E* **60**, 2037–2044 (1999).
- ⁵⁵ R. Peyret, "Introduction to high-order approximation methods for Computational Fluid Dynamics," in *Advanced Turbulent Flow Computations*, edited by R. Peyret and E. Krause (CISM, 2000), pp. 1–79.
- ⁵⁶ C. Canuto, M. Hussaini, A. Quarteroni, and T. A. Zang, *Spectral Methods in Fluid Dynamics* (Springer, New York, 1988).
- ⁵⁷ J. Shen, "Efficient spectral-Galerkin method I. Direct solvers of second- and fourth-order equations using Legendre polynomials," *SIAM J. Sci. Comput.* **15**(6), 1489–1505 (1994).
- ⁵⁸ Q. Kang, D. Zhang, and S. Chen, "Displacement of a two-dimensional immiscible droplet in a channel," *Phys. Fluids* **14**(9), 3203–3214 (2002).
- ⁵⁹ A. Lamorgese and R. Mauri, "Buoyancy-driven detachment of a wall-bound pendant drop: Interface shape at pinchoff and nonequilibrium surface tension," *Phys. Rev. E* **92**(3), 032401 (2015).